Supporting information for:

Inducing Porosity in Xylose-derived FeNC Electrocatalysts for Alkaline Oxygen Reduction

Lorenzo Mazzoli,[a] Angus Pedersen,[a,b*] Simon Kellner,[a] Robert D. Hunter,[a] Rongsheng Cai,[c] Mengnan Wang,[a] Kevin Sivula,[d] Sarah J. Haigh,[c] and Jesús Barrio[a*]

a. Department of Chemical Engineering, Imperial College London, London SW7 2AZ, UK
b. Department of Materials, Royal School of Mines, Imperial College London, London SW7 2AZ, UK
c. Department of Materials, University of Manchester, Oxford Road, Manchester, M13 9PL UK
d. Laboratory for Molecular Engineering of Optoelectronic Nanomaterials, Institute of Chemical Sciences and Engineering, École Polytechnique Fédérale de Lausanne, 1015 Lausanne, Switzerland

Experimental Section

Gas Diffusion Electrodes (GDEs) of FeXK were manufactured in-house manually with an airbrush set (Paasche) powered by an Iwata Smart Jet Pro Airbrush compressor. The GDE with the Pajarito catalyst was prepared via an Exactacoat (Sonotek) ultrasonic spraycoater with a 48 kHz nozzle at 0.15 mL min^{-1} (air shaping 0.3 psi) with an offset serpentine spray pattern on a 5 cm^2 gas diffusion layer (Freudenberg H23C8) while heated at 40°C on a vacuum plate. The gas diffusion layer was weighed pre and post-cathode catalyst spraying to determine the cathode catalyst loading. The ink formulation for GDE production consisted of a total solid content of 10 mg in a solvent mixture comprising 50.7 mL of Sustainion (in 5% ethanol) and 4.94 mL of ethanol. Subsequently, the glass vials containing the catalyst inks were immersed in an ultrasonic ice bath and subjected to sonication for a duration of 30 minutes; the compounds were then left stirring overnight. Circular areas of Freudenberg H23C8 with a 2 cm diameter are exposed during the spraying, which are dried at a hot plate during the spraying at a temperature of 60 °C. For measurement a 3 mm diameter piece of the GDE is punched out of the sprayed 2 cm diameter and inserted into a 3 mm diameter hole of a H23C8 carbon, which is positioned exactly underneath the hole of the upper cell body for the working electrode area.[1] Then a Sustainion X37-50 Grade 60 membrane of 2 cm diameter is placed above the H23C8 carbon with the catalyst layer. The upper cell body is screwed onto the lower cell body applying pressure onto the membrane and catalyst layer. The lower cell body with flow-field facing towards the H23C8 carbon paper is connected to a bubbler to humidify the reactant gas before it reaches the GDE. The hydrogen reference electrode was manufactured in-house and the hydrogen in the capillary is prepared freshly before each single catalyst layer testing. The hydrogen reference electrode is located in a luggin capillary, which is in contact with the Sustainion membrane via a small hole located 2 mm next to the hole for the working electrode area. The chosen counter electrode was a Pt coil. All electrochemical measurements were conducted at room temperature using a potentiostat PGSTAT204 with FRA32M Module (Metrohm) in combination with a BOOSTER10A. The upper cell compartment of the Gas Diffusion Electrode (GDE) setup was filled with a 1 M KOH aqueous solution. To prepare for the measurements, the catalyst layer was conditioned by subjecting it to potential cycling between 0.06 and 1.10 V vs. the reversible hydrogen electrode (V_{RHE}) in nitrogen atmosphere until a stable cyclic voltammogram was observed. This process typically involved around 10 cycles at a scan rate of 50 mV s^{-1} and 15 cycles at a scan rate of 500 mV s^{-1}. Prior to commencing measurements, the working electrode (WE) was subjected to an open circuit potential (OCP) gas purge with a flow rate of 200 ml min^{-1} of humidified O_2 for a duration of 10 minutes. Subsequently, galvanostatic steps coupled with Electrochemical Impedance Spectroscopy (EIS) were employed. During this phase, the gas purge flow rate remained at 200 ml min^{-1} of O_2 at ambient pressure. Current steps were applied, with corresponding hold times, including -0.1 mA cm^{-2} (90 seconds) -1/-2.5 mA cm^{-2}, -5/-10 mA cm^{-2} (30 seconds), and -25/-50/-100/-250 mA cm^{-2} (5 seconds), followed by -0.5/-1.0/-1.5/-2.0 A cm^{-2} (5 seconds). At each step, an EIS was recorded for 100% post-correction. The value for the uncompensated resistance is from the magnitude of the impedance, for which the phase angle is closest to 0 in the high-frequency region > 1000 Hz. The results were normalized to the catalyst loadings of 1.29 and 1.05 $mg_{Catalyst}$ cm^{-2}, respectively, for PMF-D14401 and FeXK.

Materials Characterization.

Nitrogen sorption measurements were carried out in a Micromeritics 3Flex system at -196 °C with a pressure range from 10^{-5} to 0.99 p/p^0. The specific surface area was calculated by the BET Surface Identification software, by only taking increasing values, in a pressure range usually below 0.3.[2] The pore size distribution was determined using the Heterogeneous 2D Carbon Surface non-local density functional theory NLDFT N_2 77 K method, which involved analyzing the adsorption segments of the isothermal data. This method was applied due to incorporation of more realistic geometric corrugation and energetical heterogeneity in the surface of the carbon, which limits artifacts in the pore size distribution.[3] Scanning electron microscopy (SEM) was conducted on Zeiss Leo Gemini 1525 with a thin layer of chromium sputtered onto the specimen surface owing to the lack of conductivity. X-ray diffraction (XRD) patterns were obtained with a PANalytical X'PERT PRO powder X-ray diffractometer using a Cu Kα source operating at 45 kV and 30 mA. The scan step size was set to 0.033°. X-ray photoelectron spectroscopy (XPS) analysis was performed using a Thermo Fisher K-Alpha XPS system, and the acquired spectra were analyzed utilizing the Avantage software. To account for charging effects, all spectra were calibrated relative to the carbon C1s peak at 284.8 eV. Inductively coupled plasma mass spectrometry (ICP-MS) analysis was conducted using an Agilent 7900 spectrometer (Agilent Technologies). For the ICP-MS analysis, approximately 3-5 mg of the material was digested in aqua regia, consisting of 25% v/v HNO_3 (70%, Certified AR, Eur.Ph., for analysis Fisher Chemical, Fisher Scientific) and 75% v/v HCl (37%, Certified AR, Eur.Ph., for analysis Fisher Chemical, Fisher Scientific), employing a MARS 6 microwave at 1,500 W for 15 minutes at 215 °C. The resulting solutions were diluted 20 times and measured against calibration standards containing Fe concentrations of 0, 2, 50, 100, 200, and 500 ppb. The morphology and chemical composition of the catalysts were characterized by scanning transmission electron microscopy (STEM) and energy dispersive X-ray spectroscopy (EDX) using a Thermo Fisher Titan STEM (G2 80–200) equipped with a Cs probe corrector (CEOS) and a high-angle annular dark-field (HAADF) detector, operating at 200 kV. The TEM samples were prepared by dispersing the catalyst powders into a methanol solution followed by drop-casting the solution onto a copper grid coated with an amorphous holey carbon film. Raman spectra were collected on a Renishaw inVia micro-Raman (500-3200 cm^{-1}), using a 50 mW

Comment [PA]: @Lorenzo - please add ref: J. Jagiello, J. P. Olivier, Adsorption 2013, 19, 777 laser with a wavelength of 532 nm at 10% laser power. Samples were prepared by drop casting in ethanol onto a glass slide. Statistical Raman data were obtained from maps of 25 areas per sample. The first-order spectra were deconvoluted using a 4-point fitting model consisting of Voigtian functions. FT-IR spectra were collected in attenuated total reflectance mode in an Agilent Cary 630 FRIF spectrometer. 32 Background and sample scans were employed.

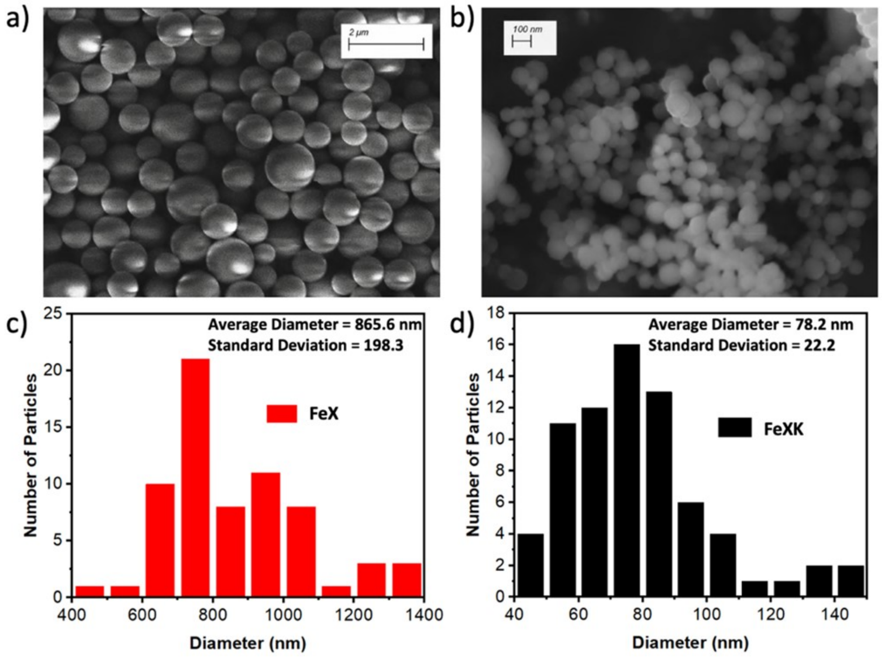

Figure S1. SEM images and particle size distribution histograms of HTC-X (a, c) and HTC-XK (b,d)

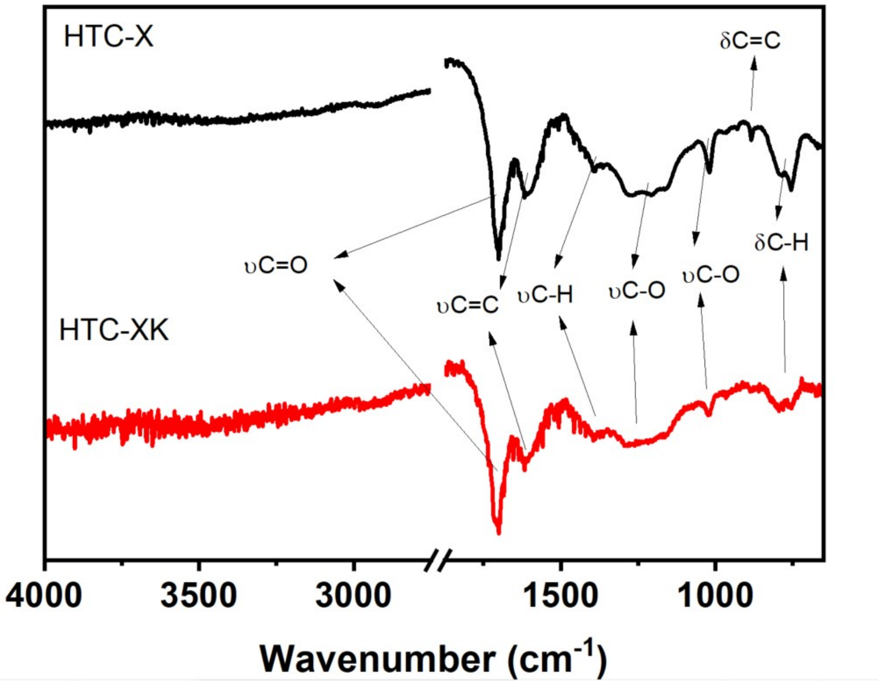

Figure S2. FTIR Spectra of FeX and FeXK

Table S1. N_2 sorption parameters, including specific surface area, pore volumes and micropore percentage.

Sample	BET Specific Surface Area ($m^2\ g^{-1}$)	Micropore Volume ($cm^3\ g^{-1}$)	Mesopore Volume ($cm^3\ g^{-1}$)	Micropore volume (%)
FeXK	478	0.179	0.138	57
FeX	127	0.045	0.037	55

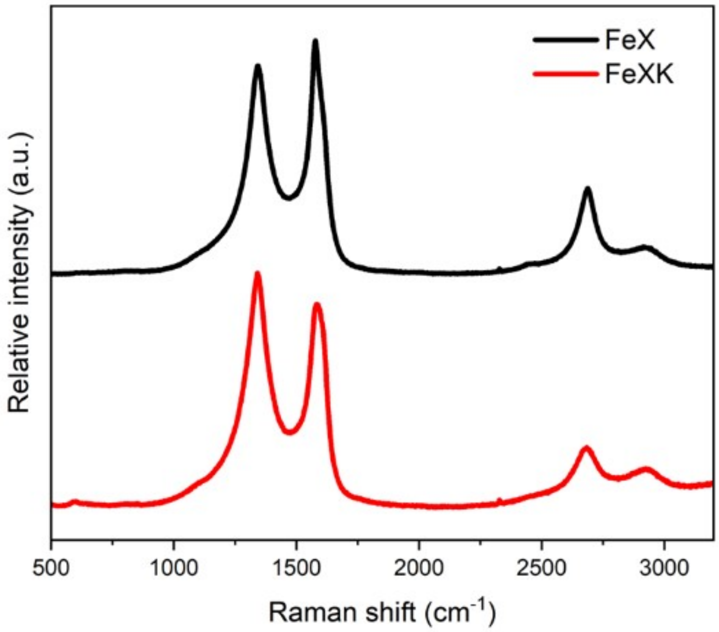

Figure S3: Raman spectra of FeX and FeXK

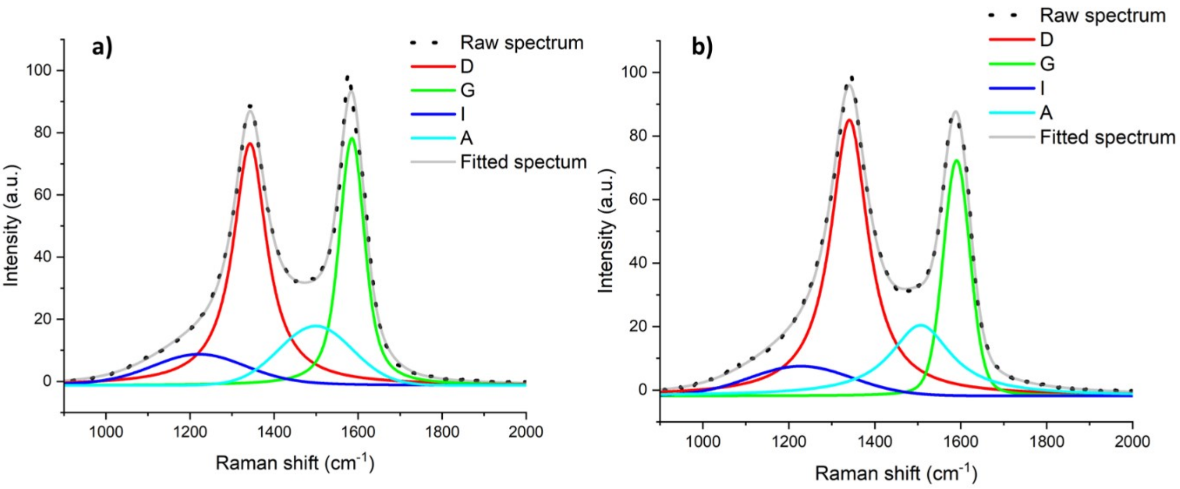

Figure S4: Example of deconvoluted Raman spectra for a) FeX and b) FeXK.

Sample	I_D/I_G
FeX	1.03 +/- 0.17
FeXK	1.15 +/- 0.05

Table S2: ID/IG ratios derived from deconvolution of Raman spectra. Measurements were collected at 25 different locations and the average values are reported with standard deviations.

Deconvolution of Raman spectra was performed using 4 Voigt peaks. The additional bands, I and A, used in the deconvolution procedure were ascribed to polyene-like structures[4] and amorphous carbon respectively.[5]

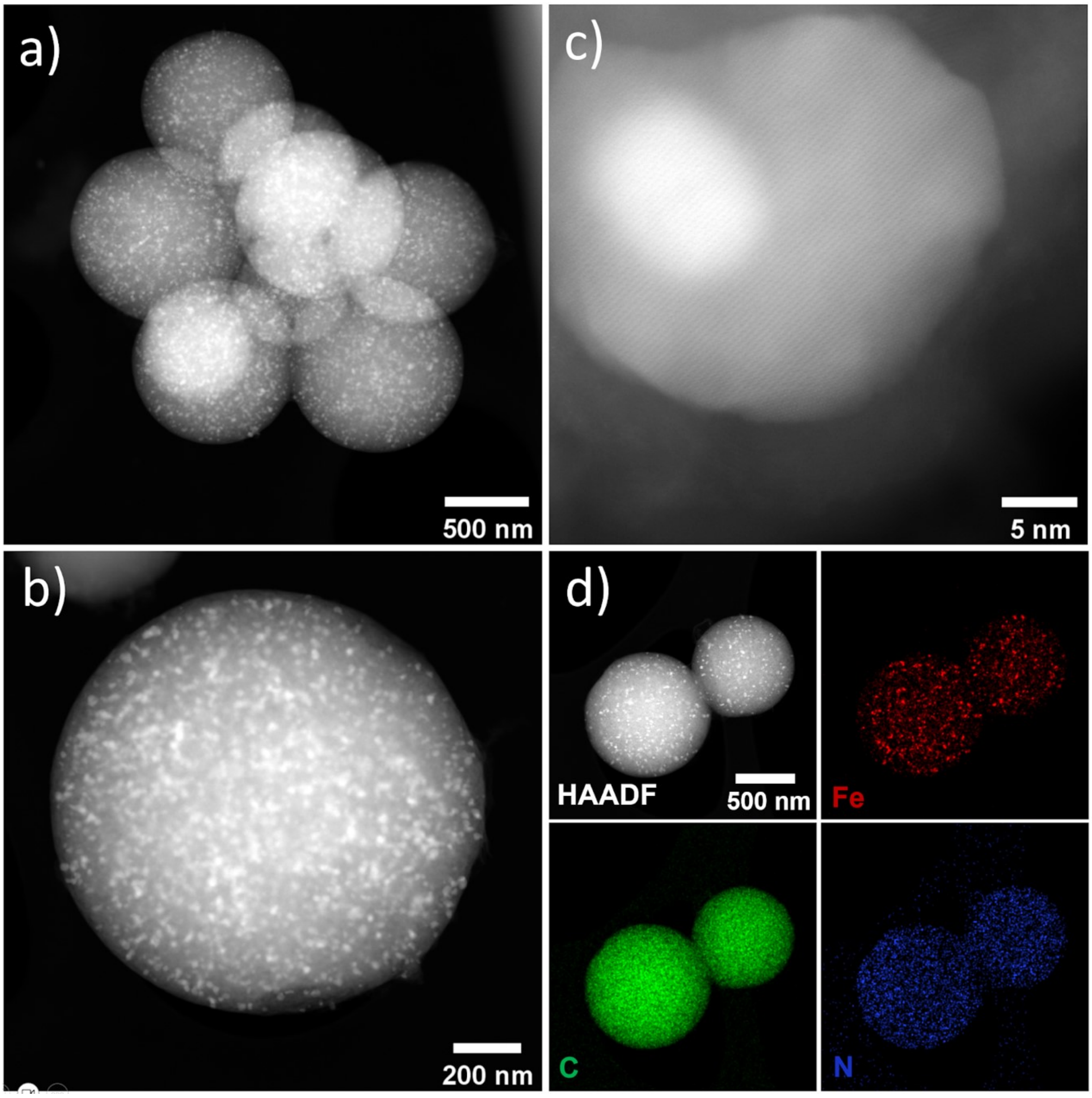

Figure S5. HAADF-STEM images showing distributed Fe-based particles (a-b, d-f) and EDX elemental maps for C (green), Fe (red), and N (blue) (c) of FeX.

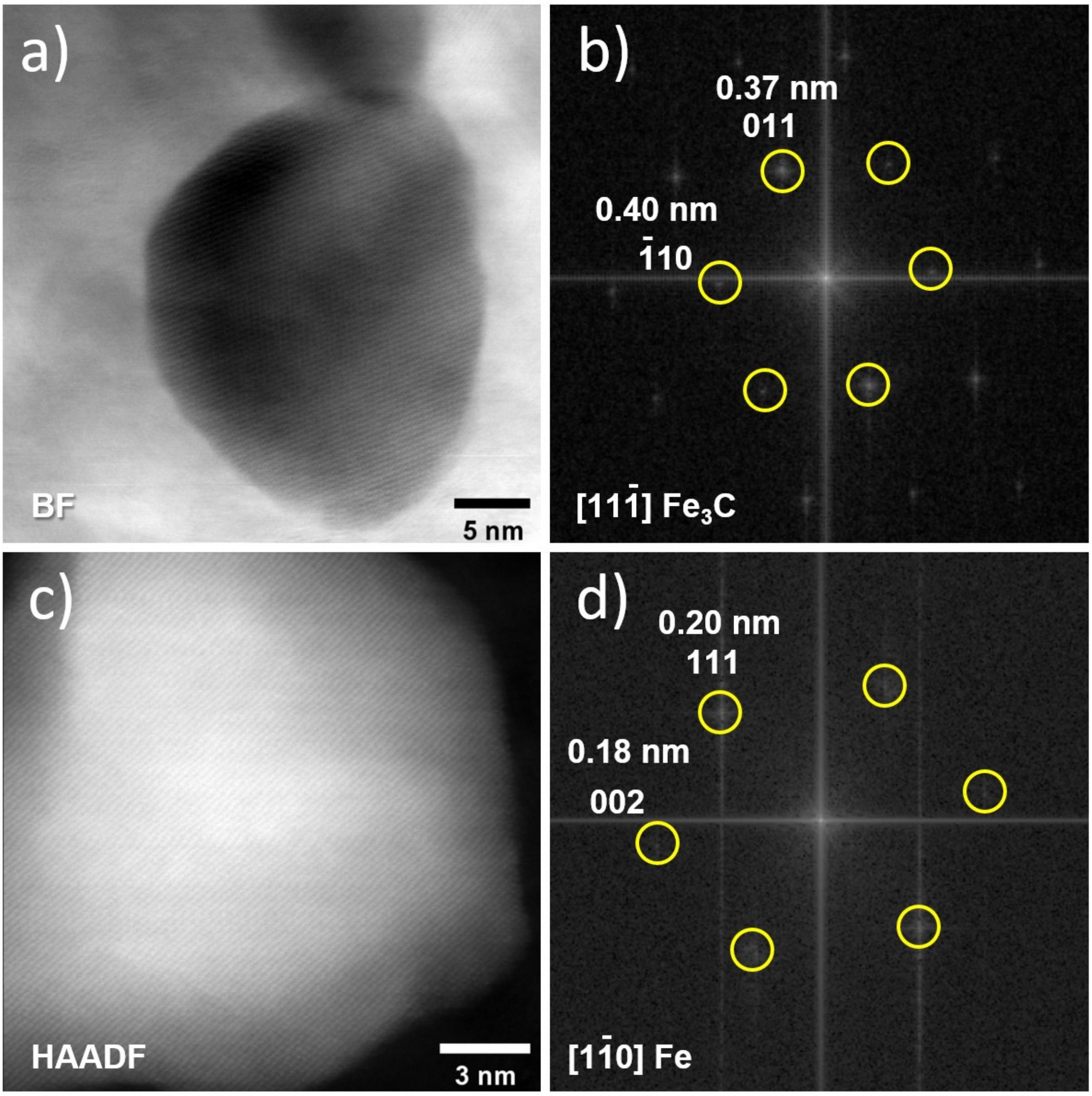

Figure S6: STEM images and corresponding FFT with assigned Miller indices of crystal planes for particles identified in a, b) FeX and c, d) FeXK.

Table S3. Chemical composition from XPS analysis for FeX(a) and FeXK (b).

Sample name	C1s wt%	N1s wt%	O1s wt%	Fe2p wt%	C1s at%	N1s at%	O1s at%	Fe2p at%
FeX	79.0	11.4	6.5	3.11	83.8	10.4	5.15	0.71
FeXK	90.2	3.55	4.77	1.46	92.9	3.13	3.36	0.32

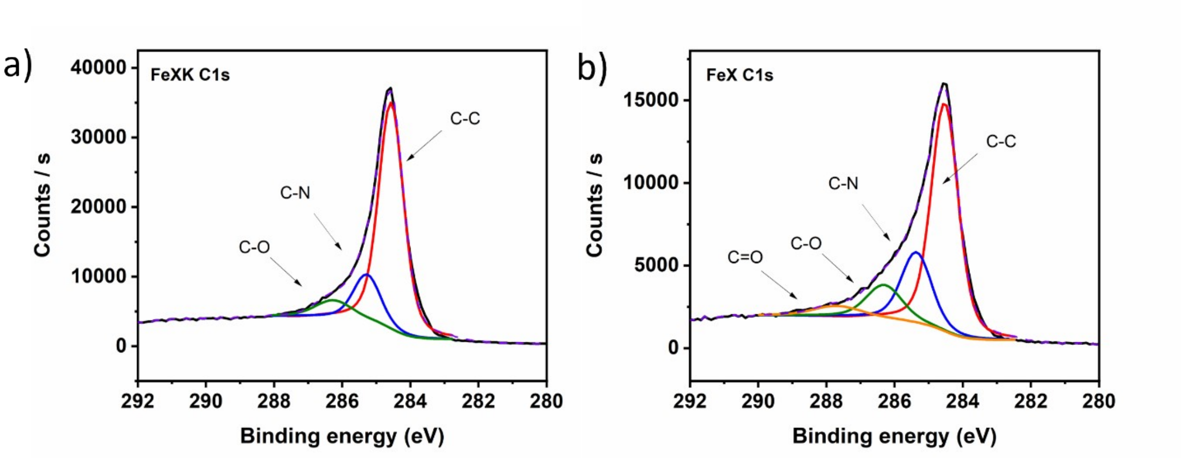

Figure S7. C1s XPS spectrum for FeX(a) and FeXK (b).

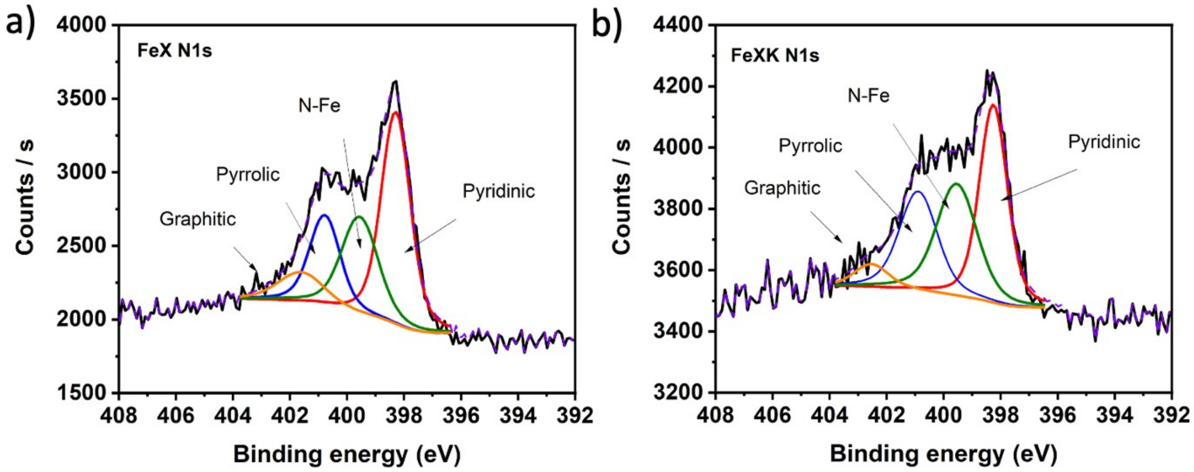

Figure S8. N1s XPS spectrum for FeX(a) and FeXK (b).

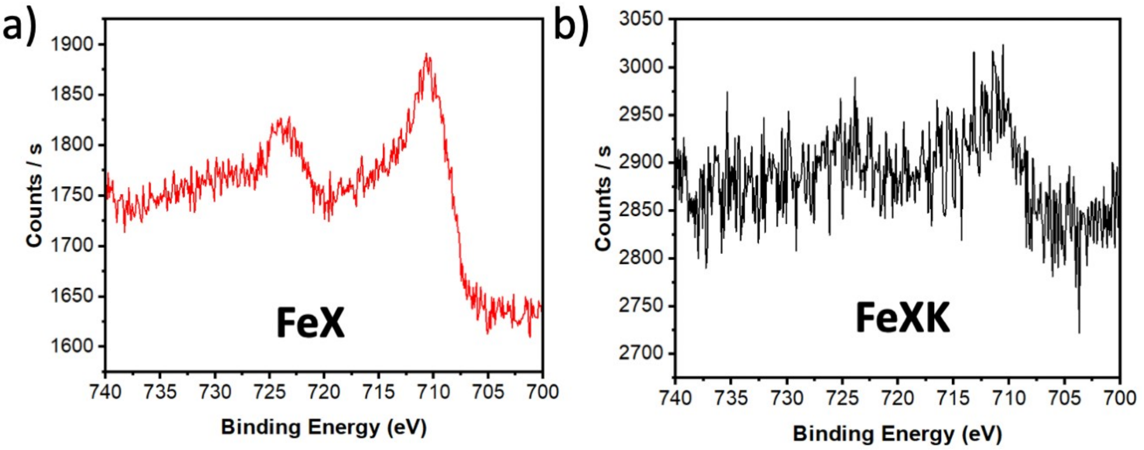

Figure S9. Fe2p XPS spectrum for FeX(a) and FeXK (b).

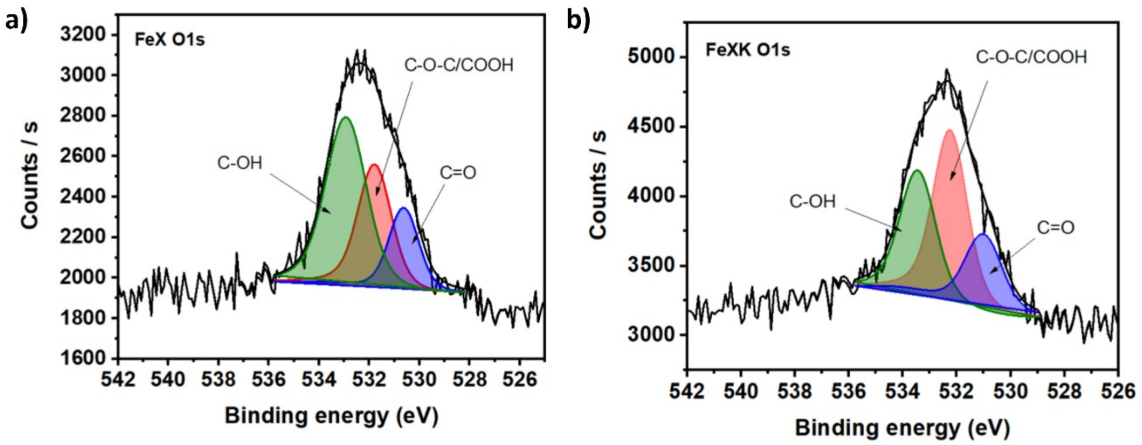

Figure S10. O1s XPS spectrum for FeX(a) and FeXK (b).

Table S4. Atomic percentage of the different O1s XPS species in FeX and FeXK

Bond type	FeX at %	FeXK at%
C=O	18.9	28.1
C-O-C/COOH	30.9	34.1
C-OH	50.2	37.8

Table S5. Kinetic performances of electrocatalysts measured in this work

Sample	J_d at 0.80V (mA cm^{-2})	J_{lim} (mA cm^{-2})	J_{kin} at 0.80V (mA cm^{-2})	Loading (mg cm-^{2})	m_{kin} (A g^{-1})
FeXK	-2.19	-5.36	-3.71	0.26	14.30
FeX	-0.34	-3.68	-0.36	0.26	1.45
PMFD14401	-3.28	-4.96	-9.76	0.26	37.53

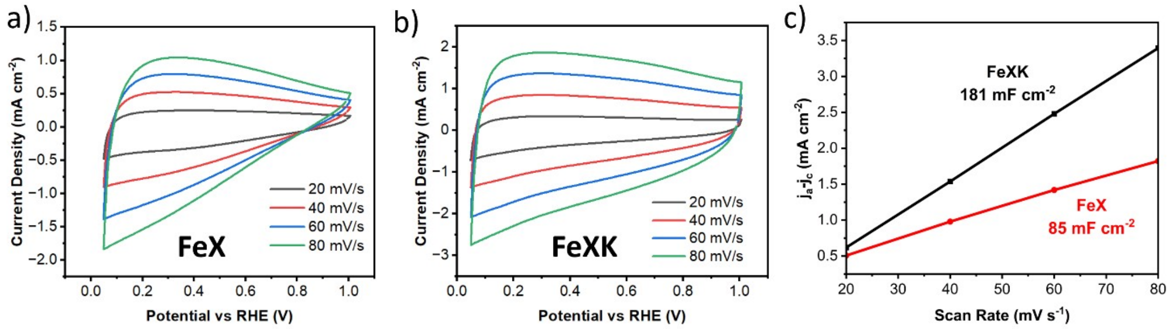

Figure S11. RRDE capacitive measurements at different scan rates in KOH 0.1 M, 0 rpm, in N_2, with a 0.26 mg cm^{-2} loading of a) FeNCS@ b) FeXK@. c) (j_a-j_c) vs scan rate plot, and C_{dl} (from slope value) at 0.5 V vs RHE.

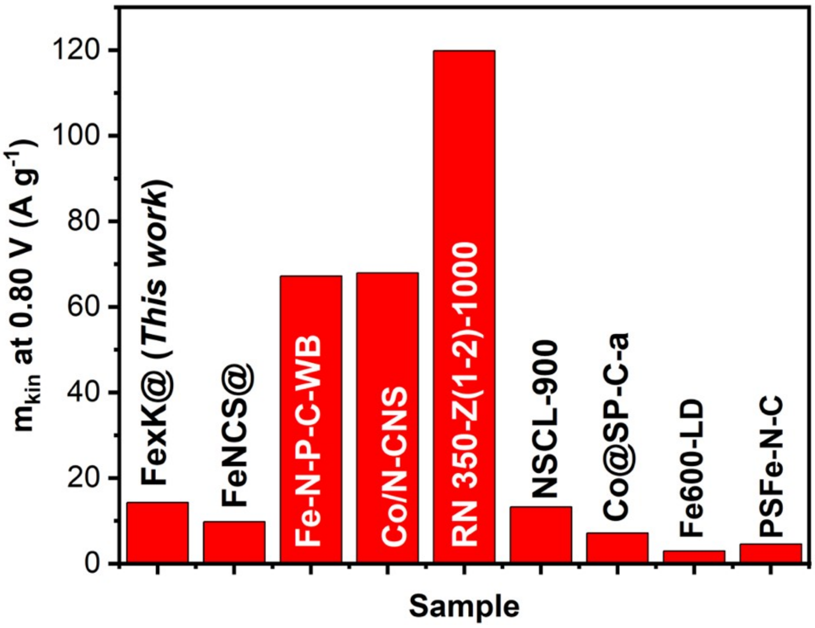

Figure S12. Kinetic Mass Activities at 0.80 V_{RHE} of some biomass-derived catalysts from the literature.

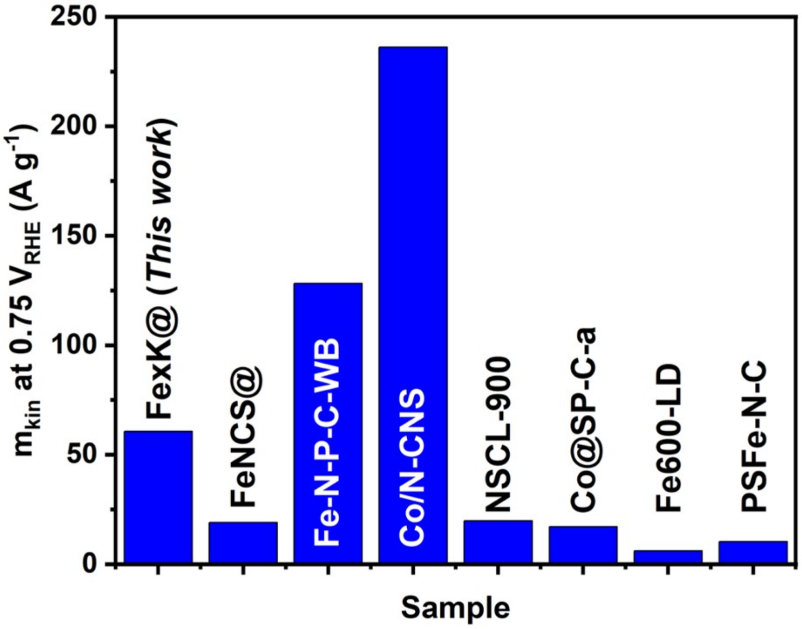

Figure S13. Kinetic Mass Activities at 0.75 V_{RHE} of some biomass-derived catalysts from the literature

We would like to note that, while more biomass-derived catalysts have been reported in most cases the employed setup or procedure was often not specified nor suitable for using the catalyst as an appropriate comparison, either because the catalyst loading was not specified, the counter electrode in the RRDE setup was Pt-based (by using Pt, the performances of the catalysts are highly influenced by the presence of the noble metal, delivering, therefore, better results), or working electrode surface not mentioned in the paper. In other cases, just metrics such as half-wave potential, on-set potential, and limiting current density were employed which are dependent on the mass loading and cannot therefore be used as univalent comparative instruments. This Table was therefore created by selecting those few catalysts that were found to be tested in an alkaline electrolyte with a non-noble metal counter electrode and calculating the kinetic mass activity.

Table S6. Summary of ORR performances of some biomass-derived catalysts from literature, measured with appropriate RRDE setup.

Biomass Source	Other Sources	Synthesis Method	SSA (m^2 g^{-1})	Current Density at 0.80 V (mA cm^{-2})	Limiting Current Density (mA cm^{-2})	Kinetic Current Density at 0.80 V (mA cm^{-2})	Kinetic Mass Activity at 0.80 V (A g^{-1})	Ref
Wood Briquettes	$FeCl_3$ H_3PO_4	Impregnation, Pyrolysis	1608	-4.8	-5.6	-33.60	67.20	6
Vitamin B2	NaCl Co (OAc)_24H2O	Lyophilization, pyrolysis	513	-3.8	-4.7	-19.84	67.96	7

Root nodules	$ZnCl_2$	Carbonization, activation, pyrolysis	1838	-4.3	-5.24	-23.97	119.85	8
Walnut Shell	Urea, $g-C_3N_4$	Activation, pyrolysis	-	-1.51	-2.78	-3.30	13.22	9
Soybean	Zinc nitrate hexahydrate, cobalt(II) nitrate hexahydrate, potassium hydroxide (KCl)	Impregnation, pyrolysis	331.59	-1.6	-6.13	-2.16	7.15	10
Litchi-derived	KOH, metal phthalocyanine	Activation, two pyrolysis	-	-1.28	-4.7	-1.75	2.93	11
Peach stones	Urea, Iron Nitrate	Impregnation, two pyrolysis	846	-1.51	-4.5	-2.27	4.54	12
Xylose	Melamine, $FeCl_2$	Impregnation, Pyrolysis	70	-1.65	-4.17	-2.74	9.80	13
Xylose (This Work)	Kayexalate, Melamine, $FeCl_2$	Impregnation, Activation, Pyrolysis	478	-2.19	-5.36	-3.71	14.30	This Work

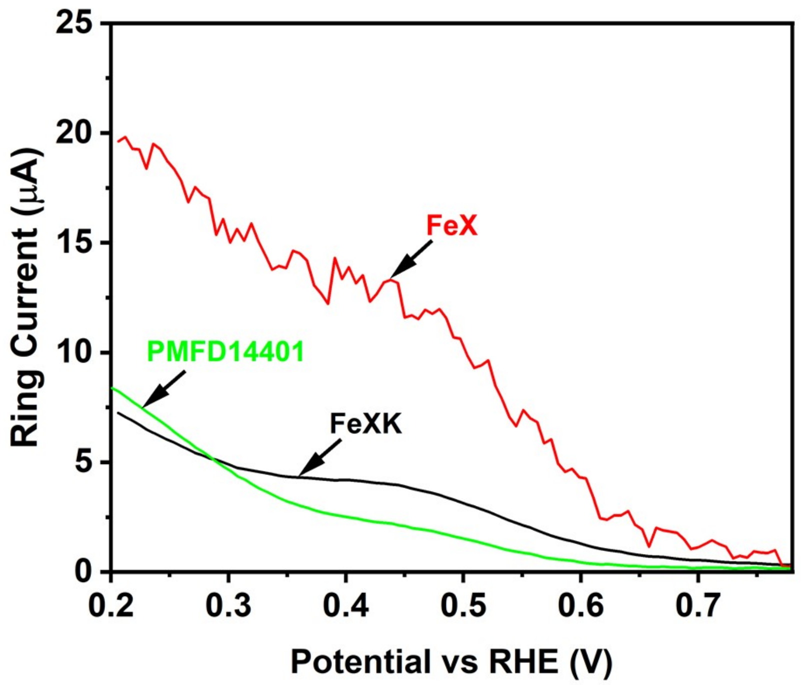

Figure S14. Cathodic potentiostatic curve of Pt ring current (held at 1.27 V_{RHE}) versus potential for FeX, FeXK and PMFD14401 under 1600 rpm in O_2-saturated 0.1 M KOH.

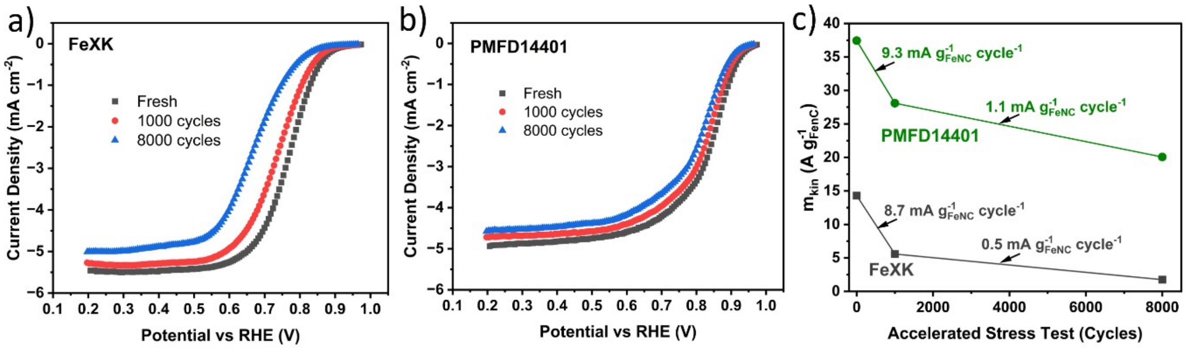

Figure S15. O_2 reduction current density from cathodic scan RRDE measurements for fresh and after 1000 and 8000 accelerated stress test cyclic voltammetry cycles (0.8-0.4 V_{RHE} at 100 mV s^{-1} under O_2-saturation in 0.1 M KOH with Pt ring applied at 1.27 V_{RHE} throughout), for a) FeXK and b) PMF-D14401. Corresponding change in kinetic mass activity for FeXK and PMFD14401 c).

References

1 G. K. H. Wiberg, S. Nösberger and M. Arenz, *Curr. Opin. Electrochem.*, 2022, **36**, 101129.

2 *ISO 9277*, 2022.

3 J. Jagiello, C. Ania, J. B. Parra and C. Cook, *Carbon N. Y.*, 2015, **91**, 330–337.

4 B. Dippel, H. Jander and J. Heintzenberg, *Phys. Chem. Chem. Phys.*, 1999, **1**, 4707–4712.

5 A. Sadezky, H. Muckenhuber, H. Grothe, R. Niessner and U. Pöschl, *Carbon N. Y.*, 2005, **43**, 1731–1742.

6 Y. Li, K. Zang, X. Duan, J. Luo and D. Chen, *J. Energy Chem.*, 2021, **55**, 572–579.

7 Y. Zheng, S. Chen, H. Lu, C. Zhang and T. Liu, *Nanotechnology*, 2020, **31**, 364003.

8 M. Hao, R. Dun, Y. Su, L. He, F. Ning, X. Zhou and W. Li, *J. Mater. Chem. A*, 2021, **9**, 14331–14343.

9 L. Yan, Y. Liu and J. Hou, *Molecules*, , DOI:10.3390/molecules28052072.

10 Y. Wu, Q. Hou, F. Li, Y. Sang, M. Hao, X. Tang, F. Qiu and H. Zhang, *Catalysts*, , DOI:10.3390/catal13071118.

11 S. A. Mirshokraee, M. Muhyuddin, R. Lorenzi, G. Tseberlidis, C. Lo Vecchio, V. Baglio, E. Berretti, A. Lavacchi and C. Santoro, *SusMat*, 2023, **3**, 248–262.

12 S. Pérez-Rodríguez, D. Sebastián, C. Alegre, T. Tsoncheva, N. Petrov, D. Paneva and M. J. Lázaro, *Electrochim. Acta*, 2021, **387**, 138490.

13 J. Feng, R. Cai, E. Magliocca, H. Luo, L. Higgins, G. L. F. Romario, X. Liang, A. Pedersen, Z. Xu, Z. Guo, A. Periasamy, D. Brett, T. S. Miller, S. J. Haigh, B. Mishra and M. M. Titirici, *Adv. Funct. Mater.*, , DOI:10.1002/adfm.202102974.